Nanoscale

PAPER

View Article Online
View Journal

Cite this: DOI: 10.1039/d1nr04790f

Single GaP nanowire nonlinear characterization with the aid of an optical trap†

Alexey D. Bolshakov, *[a,b,c] Ivan Shishkin,[c,d] Andrey Machnev,[d] Mihail Petrov,[c] Demid A. Kirilenko,[c,e] Vladimir V. Fedorov,[a,f] Ivan S. Mukhin[a,c,f] and Pavel Ginzburg[b,d]

Semiconductor nanowires exhibit numerous capabilities to advance the development of future optoelectronic devices. Among the III–V material family, gallium phosphide (GaP) is an attractive platform with low optical absorption and high nonlinear susceptibility, making it especially promising for nanophotonic applications. However, investigation of single nanostructures and their waveguiding properties remains challenging owing to typically planar experimental arrangements. Here we study the linear and nonlinear waveguiding optical properties of a single GaP nanowire in a special experimental layout, where an optically trapped structure is aligned along its major axis. We demonstrate efficient second harmonic generation in individual nanowires and unravel phase matching conditions, linking between linear guiding properties of the structure and its nonlinear tensorial susceptibility. The capability to pick up single nanowires, sort them with the aid of optomechanical manipulation and accurately position pre-tested structures opens a new avenue for the generation of optoelectronic origami-type devices.

Received 23rd July 2021,
Accepted 29th November 2021

DOI: 10.1039/d1nr04790f

rsc.li/nanoscale

Introduction

Continuous endeavours in the miniaturization of photonic devices have promoted the use of single nanostructures as functional elements in future circuitry. While quite a few architectures have been proposed, nanowires (NWs) serve as a compromise between zero- and two-dimensional heterostructures. Being compact on one hand and electrically and optically accessible on the other hand, NWs have been demonstrated as a promising platform for single photon emitters,[1] detectors and converters,[2] nonlinear gates and many others.[3,4]

Among a variety of compound semiconductors, III–V materials have distinctive advantages, including flexible bandgap engineering[5,6] and tailor-made electrical properties.[7] In particular, the reduced dimensionality of III–V NWs allows one to greatly expand their functionalities compared to the conventional thin-film heterostructures including growth on lattice-mismatched substrates and novel abilities for bandgap engineering *via* controlled syntheses of metastable crystal phases.[8]

Typically, III–V NWs are synthesized by epitaxial techniques on either native or silicon (Si) substrates.[9] In both cases, fabrication of a photonic device and studying the optical properties of the as-grown NWs are limited due to a low optical contrast between the NWs and substrates, making optical leakages rather pronounced.[10,11] However, owing to their small footprints, NWs can be easily mechanically cleaved from the growth substrate and transferred onto an "optical contrast" wafer, *e.g.* glass. Planarization of NWs allows their future integration in large-scale photonic circuitry. In terms of single wire optical characterization, this layout enables performing a scan along the structure, which is beneficial for analyzing photoluminescence (PL), Raman and dark-field responses of an isolated element. On the other hand, this planar experimental arrangement significantly complicates the excitation along the wire's axis, which allows probing the linear and nonlinear properties and governing the waveguiding scenarios. For example, longitudinal resonances, nonlinear harmonic generation, Raman signatures and many others strongly depend on the optical guiding properties of the wire. An experimental geometry for those investigations can be realized with NW encapsulation into an optically transparent polymer matrix with subsequent detachment from the growth substrate.[12] This approach, however, being of pure modularity, causes severe difficulties in subsequent spectroscopic studies owing to a small NW cross section, limiting its individual excitation in the vertical direction with the aid of optical microscopy.

[a]Alferov University (formerly St Petersburg Academic University), 194021 St Petersburg, Russia. E-mail: bolshakov@live.com
[b]Centre for Photonics and Two-Dimensional Materials, Moscow Institute of Physics and Technology, 141701 Dolgoprudny, Russia
[c]ITMO University, 197101 St Petersburg, Russia
[d]Department of Electrical Engineering Tel Aviv University Ramat Aviv, Tel Aviv 69978, Israel
[e]Ioffe Institute, Saint-Petersburg, 194021, Russia
[f]Peter the Great St Petersburg Polytechnic University, 195251 St.Petersburg, Russia

†Electronic supplementary information (ESI) available. See DOI: 10.1039/d1nr04790f

Consequently, developing new tools for single wire characterization will be quite beneficial.

Optomechanical tweezing,[13] being initially applied on spherical objects with a biological outlook,[14] became a powerful tool for nanostructure manipulation. During the last few decades a large variety of nontrivial geometries, realized in quite a few material platforms, have been demonstrated and considered for numerous applications, *e.g.*,[15–17] optomechanical manipulation of NWs has been demonstrated in several reports with a primary goal to study fluid interactions, *e.g.*,[18] holographic optical tweezers were shown to provide single NWs with superior trapping capabilities.[19] Optical trapping can be performed with either continuous wave (CW) or pulsed laser radiation. While an averaged laser power governs a mechanical motion (in the case of an overdamped motion in a fluid), nonlinear optical interactions can emerge under moderately high energy excitation with ultra-short pulses. In this case, optical trapping of a NW with femtosecond (FS) laser pulses allows for a simultaneous alignment of the structure along the optical axis and its efficient nonlinear excitation. For example, an optically trapped individual potassium niobate ($KNbO_3$) NW, acting as an efficient local second harmonic (SH) generator, was demonstrated in ref. 20, opening new pathways for optical microscopy with sub-wavelength resolution. The nonlinear optical properties of single alkaline niobate NWs were extensively studied in ref. 21, demonstrating strong SH generation.

Microphotoluminescence, combined with optical trapping, was used for the optical characterization of a single InP NW in ref. 22. Structural studies, important for the investigation of the NW crystallinity, were performed *via* analysis of the local photoluminescence (PL) response. An accurate alignment of NWs along the trapping beam optical axis maximized the PL signal and light collection. An efficient nonlinear optical response and PL, stimulated by two-photon absorption from a single trapped InP NW, were demonstrated experimentally in ref. 23.

While several investigations of optically trapped wires have been performed, quite a few important aspects were overlooked. For example, the impact of the NW geometry on the nonlinear generation efficiency was not explored. Here we perform comprehensive studies of optically trapped gallium phosphide (GaP) NWs. GaP is a fast-developing III–V material platform with many remarkable optical and electrical properties, making it a probable contributor to future nanophotonic circuitry. In particular, GaP exhibits a broad transparency window (0.5–11 μm),[24] high thermal conductivity (70–100 W m^{-1} K^{-1}) at 300 K, and a large value of the quadratic nonlinear susceptibility (~70 pm/V@1 μm).[25] It should be noted that despite a low volume, a SHG response can be significantly enhanced in nanostructures due to strong light confinement and optical resonances at fundamental or second-harmonic wavelengths. Lacking the crystalline inversion symmetry, GaP NWs have an extremely high surface to volume ratio, opening room for the tailored state of the art nonlinear optical properties that have been proved previously for several geometries such as doubly resonant (ω, 2ω) microdisks, nanopillars, *etc.*[26–29] These characteristics together with the NW heterostructure band engineering[30,31] and geometrical flexibility[32,33] make GaP NWs an attractive platform for implementation in passive and active devices, integrated with an all-dielectric nanophotonic circuitry.[34]

The focus of this report is making detailed studies on a single optically trapped GaP NW. We probe the sample with several laser sources to perform comprehensive characterization. A wideband supercontinuum white laser is used for linear spectroscopy, while a femtosecond infra-red (IR) source plays a dual role. It is introduced to trap the structure and serves as a pump for the SHG response. We explore the correlations between the NW geometry and its SHG response both experimentally and theoretically, providing an outlook on phasematching conditions and the optimization of NW geometries towards optoelectronic applications.

Experimental

Nanowire growth

Self-catalyzed GaP NWs were synthesized using a Veeco GEN III molecular beam epitaxy machine on Si (111) substrates according to the protocol reported previously.[35,36] The following growth conditions were used: a Ga flux of 1.3×10^{-7} Torr and a P_2 flux (provided by a valved cracker) of 4.2×10^{-6} Torr (corresponding to planar GaP growth with a rate of 0.4 μm h^{-1}) at a temperature of 610 °C. The scanning electron microscopy (SEM) image of the grown sample is presented in Fig. 1(a). Typical NW sizes were 10 μm in length and 175 nm in diameter. Statistical analysis of the NW dimensions will be discussed further. A typical SEM image of the planarized NWs, mechanically cleaved from the growth substrate and transferred to auxiliary wafer, is presented in Fig. 1(b). A reflection high energy electron diffraction (RHEED) pattern obtained *in situ* is presented in the Fig. 1(a) inset, and it demonstrates that NWs grow epitaxially preserving the GaP bulk cubic zinc blende (ZB) structure belonging to the $F\bar{4}3m$ space group,[37] maintaining the same crystallographic orientation as that of the Si (111) wafer. According to the previously reported structural analysis of GaP/Si(111) NWs the ZB structure lattice parameter is 5.448 ± 0.003 Å.[31]

Transmission electron microscopy (TEM) was used to study the crystallinity of the NWs (see Fig. 1(c)) with a Jeol JEM-2100F microscope (accelerating voltage 200 kV, point resolution 0.19 nm). The obtained bright-field image demonstrates multiple twinning of the ZB lattice structure along the growth ⟨111⟩ direction, typical of the self-catalyzed III–V NWs.[38] Twinned diffraction spots corresponding to the $[1\bar{1}0]_{ZB\text{-}GaP}$ and $[\bar{1}10]_{ZB\text{-}GaP}$ zone axis patterns can be found on the obtained RHEED and selected area electron micro-diffraction (SAED) patterns presented in the Fig. 1(a) inset and in Fig. 1(d), respectively. The corresponding diffraction spot positions are marked by red solid and yellow dashed circles. According to the previous study, even with numerous twinning

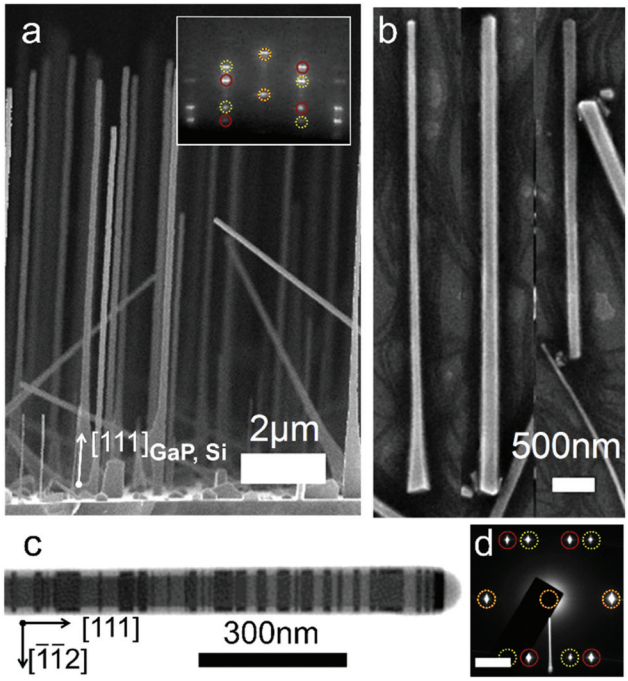

Fig. 1 Images of the synthesized NWs: SEM: (a) cross-sectional view on a sample cleaved edge (inset – RHEED pattern obtained *in situ* during the NW MBE growth) and (b) mechanically cleaved planarized NWs on the auxiliary wafer; (c) typical bright-field TEM image, and (d) selective area electron microdiffraction pattern, scale bar is 2.5 nm^{-1}, $[1\bar{1}0]_{ZB\text{-}GaP}$ and $[\bar{1}10]_{ZB\text{-}GaP}$ zone axis patterns are marked with red solid and yellow dashed circles.

defects, GaP NWs possess reproducible optical properties, sufficient for efficient waveguiding and broadband SHG.[39]

Optical trapping

For individual structure investigation, NWs were transferred to an aqueous solution by sonication of the sample. It is worth noting that the obtained solution contained NWs of different lengths caused by (i) the presence of shorter NWs on the growth substrate and (ii) uncontrolled NW breakdown during sonication (Fig. 1(b)).

The fluid cell filled with the solution was then placed in an optical tweezer setup, implemented with an inverted microscope design. The setup contains a high numerical aperture (NA) oil immersion objective, which focuses a trapping laser. Imaging systems are implemented at both upper and lower ports of the system. A schematic of the setup is presented in Fig. 2(a).

First, NWs were optically trapped with a femtosecond laser (YLMO 2 W), operating at 1030 nm, producing 150 fs pulses at 100 MHz repetition rate. Typical averaged powers, required for stable trapping, were found to range between 5 and 15 mW (typically 10 mW). This excitation power allows performing both optical trapping and analysis of the nonlinear optical properties. It is worth noting that in overdamped solutions optical trapping mainly depends on an averaged power and, hence, pulsed and CW lasers exhibit similar performances. What matters, however, is the nonlinear response, which demands short pulse excitation. Furthermore, our NWs are expected to exhibit a strong SHG response in the near-IR range, as was previously shown.[39] An auxiliary 980 nm continuous-wave laser (Thorlabs) is used in experiments for qualitative assessment of the SHG generation efficiency. An additional lens is placed in the beam path of the femtosecond laser to expand the beam size in the imaging plane of the setup. Such an arrangement is used to obtain homogeneous excitation fluence over the optical trap.

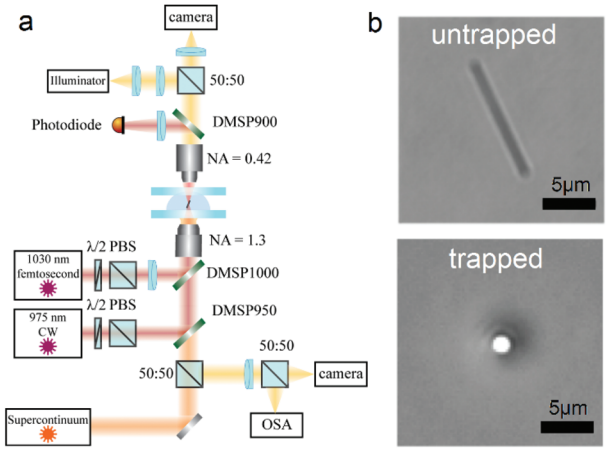

Fig. 2 (a) Optical trapping setup and (b) optical images of a GaP NW in the liquid chamber before and after trapping.

The images of a single GaP NW in the liquid chamber obtained with an optical microscope before and after trapping are presented in Fig. 2(b). As was observed during the experiment, the untrapped NW experiences Brownian motion and it is randomly oriented with respect to the microscope slide. At the same time, the trapped NW is vertically aligned along the optical axis. After the trapping, the NW can be observed as a bright spot on the camera image, indicating that light is scattered on its edge. This configuration is next to optimal for exciting waveguided modes inside the NW, as will be shown hereafter.

Results and discussion

Scattering in the freestanding NW

While the trapping laser, which is also used as a nonlinear source, has an IR spectrum, the resulting SH wavelength falls into the visible window. In order to provide an accurate description of the nonlinear generation process, the linear optical response of the NW should be investigated first. In particular, there are several major factors that influence the interpretation of the results – quality factors (*Q*-factors) of the structure at the pump and SH frequencies followed by in- and out-coupling efficiencies.

In order to study the interaction of the visible light with a single NW, backscattering spectra were collected using a spectrally filtered supercontinuum laser (YSL SC-PRO, YSL Photonics equipped with a VLF tunable filter), which was used as a source (filter band was set to 550–700 nm in order to avoid spectral overlap with the SHG signal, anticipated at

515 nm accordingly). The supercontinuum excitation intensity was adjusted using a variable neutral density filter. Backscattered light from the wire was collected with the same high NA objective and launched on a spectrometer (OSA, Avantes) using a fiber-coupled port. The acquired signal demonstrates a typical Fabry–Pérot (FP) resonance modulation, confirming that the NW acts as an optical cavity (Fig. 3(a)). The Lorentzian fit of individual dips of the signal, normalized over the laser spectrum, was used to extract the *Q*-factors of the resonances that serve as key parameters for analyzing the SHG efficiency, as demonstrated by different NWs. The estimated *Q*-factors range between 150 and 200, which was quite reasonable in the case of a rather weak lateral mode confinement. This was the consequence of the relatively small NW diameter and the elevated refractive index of the embedding medium (water). Small lateral confinement resulted in poor facet reflectivity, which in turn led to the *Q*-factor degradation. A detailed analysis, which relates the FP spectra to the wire parameters, will be done hereinafter.

SHG of the NW

Apart from the linear response of a trapped NW, the SH signal corresponding to a peak located near 515 nm can be clearly seen in Fig. 3a and originates from the IR-to-visible conversion of the trapping laser light, which serves a dual function – opto-mechanical immobilization and optical pump. To prove the second-order nonlinear nature of the response, the signal dependence on a pump-power was obtained. In our experimental setup this measurement was rather complex due to several reasons. First, the limited lifetime of the NW in the trap caused by its instability due to Brownian motion and, second, the instability of the trapping at both rather low (weak trap strength) and high pumping (possibly due to overheating followed by bubbling of the surrounding medium). Instead, the pump-power measurements were carried out with the NWs transferred onto the auxiliary glass wafer *via* direct mechanical rubbing. Glass provided high optical contrast with the NW allowing for efficient light coupling in the volume of a nanostructure. The substrate with planarized NWs was placed in the same optical setup and excited with femtosecond 1030 nm laser pulses. In order to avoid thermal effects in nonlinear measurements, the pump beam was defocused using a f = 400 mm lens, resulting in an ~20 μm spot in the imaging plane. The obtained pump-power dependence plotted on a log–log scale is presented in Fig. 3(b). A slope of 1.87 of the experimental curve was obtained by linear data fitting, corresponding to the SHG. Additional verification, related to the polarization sensitivity, is presented in the ESI, Fig. S1.†

Despite a moderately low *Q*-factor, the SHG signal was observed in most of the trapped wires. The backscattered intensity varied from wire to wire as well as the collected SHG intensity. It is worth noting that in the case of longer NWs, FP resonance was narrower than the SH linewidth, leading to the modulation of the SHG signal registered as a spectral dip in the SH peak (see Fig. S2,† ESI†). In the next section we systematically study how the geometry of a NW affects the SHG efficiency.

SHG and phase-matching within a single NW

To study the SHG quantitatively, several individual NWs were trapped consistently with a CW 980 nm ~50 mW laser and probed with a weak defocused 1030 nm femtosecond laser beam (10.2 mW power measured at the beamsplitter). Using different lasers for trapping and probing SH allows the suppression of the coupling between the optical and mechanical effects and enables studying the impact of NW dimensions on nonlinear properties quite accurately.

The SH intensity images obtained with several NWs were collected in the upper channel and recorded using a camera (typical image is presented in Fig. 4(a)). The SH intensity for each individual NW was then calculated by summing up the values of individual unsaturated pixels.

The geometry of the NW strongly affects its nonlinear optical properties. This aspect will be investigated next. The main complexity, however, is the lack of exact information on trapped NW dimensions, which cannot be extracted from the optical images. Nevertheless, the relevant information can be obtained indirectly. As was demonstrated above, the NW acts as an optical cavity, modulating the spectrum of the scattered signal. We analyze the FP modulations of the scattered signal and obtain the NW length considering $L = \frac{\lambda^2}{2\Delta\lambda(n - \lambda(\mathrm{d}n/\mathrm{d}\lambda))}$.[40] Here, L – NW length, λ – wavelength, $\Delta\lambda$ – mode spacing, and n – NW refractive index. To ensure consistency of the approach, several NWs were imaged opti-

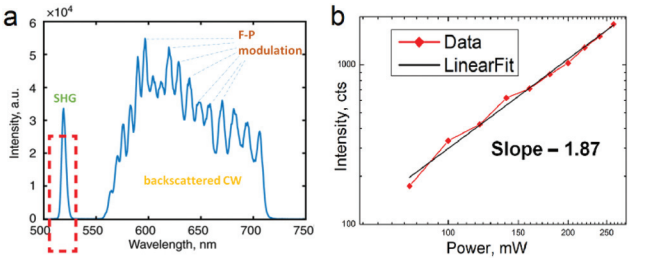

Fig. 3 (a) Backscattering response and SHG signal from an individual trapped NW and (b) SHG back-scattered signal as a function of the pump power (NW on a glass substrate).

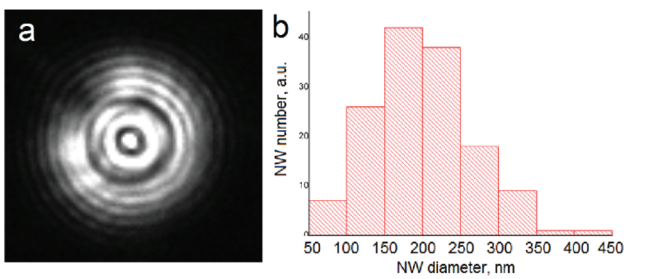

Fig. 4 (a) SH intensity image recorded using a camera and (b) statistical histogram of NW diameters.

cally prior to the trapping and then characterized with the FP formula above. The obtained results of the NW length evaluation demonstrate good convergence (ESI, Fig. S3†).

After evaluating the NW lengths, the SH intensities of several samples were measured, Fig. 5(a). The experimental data demonstrate non-monotonic dependence of the intensities on the NW lengths, indicating that other parameters might play a role. The key parameter here is the NW diameter, which has a significant impact on both linear and nonlinear properties of the wire. In the next stage, the dispersion of the NW diameters was analyzed *via* statistical studies of the planarized NW images on the Si substrate, obtained by SEM. Fig. 4(b) presents the statistical distribution of the NW diameters in the form of a histogram (not normalized probability distribution). The histogram demonstrates that the most representative NW diameters are in the 150–200 nm range with a rather pronounced dispersion, supporting the assumption of the possible influence of the NW diameter on the SHG.

To study the size effects in more detail we carried out numerical modelling of the SHG efficiency. For this purpose we implemented the so-called two-step model, using COMSOL Multiphysics.[41,42] The modelling was performed in the undepleted pump approximation, assuming that the coupling between the pump field and SH field was low and the reverse process of down-conversion could be neglected. In this case, one can analyse the nonlinear optical response in two stages – first simulating the optical response at the pump wavelength and then calculating nonlinear polarization, which acts as a source of the SH field. The optical response of the NW at the fundamental wavelength is governed by the FP resonance discussed above, which was observed in linear scattering measurements. The SH polarization distribution inside the NW was governed by the field distribution of FP modes at the fundamental wavelength and the exact form of the second order nonlinear tensor $\chi^{(2)}$:

$$P_i^{(2\omega)} = \varepsilon_0 \chi_{ijk} E_j^{(\omega)} E_k^{(\omega)} \quad (1)$$

For a monocrystalline ZB structure grown along the [111] direction coinciding with the z-axis, the nonlinearity tensor has different non-zero terms, which we will separate into two sets: (i) $\chi_{xxz}/2 = \chi_{yyz}/2 = \chi_{zxx} = \chi_{zyy} = -\chi^0/\sqrt{3}$, $\chi_{zzz} = 2\chi^0/\sqrt{3}$ and (ii) χ_{xxy}, χ_{yxx}, χ_{xxx}, χ_{xyy}. The grown NWs have a polycrystalline-twinned structure with grains having rotations with respect to the growth axis. From this perspective, the first set of $\chi^{(2)}$ tensor terms does not depend on the crystalline structure rotations, while the second set depends on the orientation of the particular grain, thus having different random values. After averaging over the random twinning grains, the second set of the terms provides a much weaker contribution to the overall SH signal, which scales linearly with the system dimensions rather than quadratically (see the ESI†).

The obtained colour map of the integral SH intensity as a function of the NW length and diameter is shown in Fig. 5(b). In the case of a cavity, the spatial overlap between the pump and SH modes governs the interaction, replacing typical phased-matching conditions, derived for propagating waves. The colour map demonstrates the range of parameters, where the generation efficiency is the highest. It is worth noting that properly chosen parameters can yield four orders of magnitude improvement with respect to samples with similar dimensions, which, however, do not grant an optimized modal overlap. A typical distribution of the pump and SH signals inside the wire in the resonance case is presented in Fig. 5(c). The most prominent response is found for 170 nm thick NWs with an overall tendency to increase the SH efficiency with the NW length.

The red curve in Fig. 5a demonstrates the numerical data on the maximum theoretical SHG efficiency (corresponding to a certain diameter where it is maximized) for a GaP NW of a given length, evaluated *via* analysis of the map in Fig. 5b. The blue curve in Fig. 5a demonstrates the minimum theoretical efficiency for the NW diameter range of 150–250 nm which corresponds to the dispersion of the NW size distribution (Fig. 4b). The obtained numerical data were used for the experimental data fitting. For a fair comparison, the numerical data were normalized to remove the impact of the signal collection efficiency. The normalization coefficient is considered constant, assuming that the difference between the numerical and experimental data is mostly governed by the aperture of the objective and should be the same for all of the data points. We chose the normalization constant such that experimental data values (i) do not exceed the theoretical maximum ones and (ii) fall in the 150–220 nm diameter range on the map in Fig. 5b satisfying the statistical distribution of the NW dimensions (Fig. 4b). Within the normalization, the SHG efficiency of a 2.5 μm long NW equals the maximum SHG efficiency for a

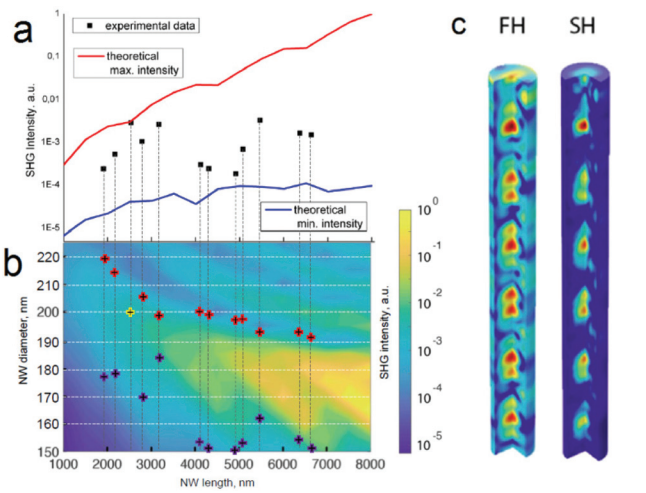

Fig. 5 (a) Experimental data on the SHG intensity as a function of the NW length (black dots) and numerically calculated maximum SHG efficiency for the given length (red curve) and minimum efficiency (blue curve). (b) Colour map of the SHG efficiency as a function of the NW length and diameter, and numerical data. Dots indicate the possible minimum (blue) and maximum (red) values of the diameter of the corresponding trapped NWs in (a). (c) Field distribution for fundamental harmonic (FH) and second harmonic (SH) waves in a resonant NW (4000 nm long and 220 nm thick).

given length which relates to a 200 nm thick NW, and the corresponding point is marked with a yellow cross on the map in Fig. 5b. The complex behaviour of the data in Fig. 5b corresponds to the interplaying impact of the wire parameters. While the diameter governs the effective modal index, the longer NW axis is responsible for the 'coherence length', linked to the SHG efficiency in the non-phased matched case. However, the 'coherence length' also depends on the effective model index mismatch, entangling width and length parameters and complicating the colormap in Fig. 5b.

Within the carried out normalization, the rest of the experimental data values are found to be a few orders of magnitude lower than the maximum theoretical values. The latter fact is a manifestation of either (i) the difference of the studied NW diameter from the value corresponding to the maximum SHG efficiency or (ii) poor signal collection due to structural and morphological features, *e.g.* NW edge geometrical peculiarities are clearly seen in Fig. 1b. NW edges can be faceted with crystal planes different from [111] after the NW breakdown from the growth substrate. In any case, the normalized data can be used to estimate the NW diameter under study. As the obtained values are different from the maximum theoretical ones, for each of the experimental data points we can find two points on the map in Fig. 5b corresponding to the given SHG efficiency and NW length. For each of the experimental points we plotted the corresponding blue (smaller diameter) and red dots (larger diameter) on the map. Considering that the collected signal can be affected by the geometry of the NW, we conclude that the real NW diameter should be in the range between the blue and red dots.

Conclusions

To conclude, here we study GaP nanowires grown on Si (111) *via* MBE. The growth protocol allowed us to synthesize nanostructures with a broad distribution of dimensions perfect for future optical characterization. For this aim, the NWs were transferred into water medium and trapped individually in the solution using the optical tweezing technique.

First, we demonstrate stable trapping with the use of femtosecond 1030 nm laser pulses providing both immobilization of the NW and excitation of the SHG. To systematically study both linear and nonlinear optical properties of NWs we trap them with a CW 980 nm laser beam and probe them with broad band 550–700 nm supercontinuum excitation and defocused 1030 nm femtosecond pulses. The approach allows registering a linear scattering response providing information on the longitudinal dimensions of the NW acting as a FP cavity and exciting the SHG and comparing the nonlinear response from different individual NWs.

The obtained experimental data demonstrate no direct correlation between the NW length and efficiency of the SHG. To study the effect in detail we provide numerical modeling, demonstrating a strong effect on the SHG of both NW dimensions: length and diameter. The phenomenon is discussed in terms of the occurrence of the NW resonance properties both for fundamental and SH with certain dimensions. The analysis of the numerical data demonstrates fast decay of the SHG by several orders of magnitude with a slight variation of the diameter by only a few tens of nanometers from the resonance value. While GaP NWs were studied in this report, other material platforms can be investigated with the aid of tools, which were developed here.

Thus, an optical trap is demonstrated to be a powerful tool for single nanostructure analysis of linear and nonlinear optical properties with the use of several probing signals. Experimental and numerical data show the importance of the precise choice of the nanostructure dimensions for achieving an efficient nonlinear response for future implementation in optical devices and advanced photonic circuitry.

Author contributions

The manuscript was written through contributions of all authors. All authors have given approval to the final version of the manuscript.

Conflicts of interest

There are no conflicts to declare.

Acknowledgements

A. D. B. would like to thank Olga Yu. Koval and Georgiy A. Sapunov of Alferov university for their help in the interpretation of the statistical data on nanowire dimensions. A. D. B. acknowledges the financial support for the optical experiments from the Russian Science Foundation (Grant No. 20-72-10192). Analysis of the experimental data is supported by the Ministry of Science and Higher Education of the Russian Federation (Grant FSRM-2020-00011). The numerical simulations have been performed in the framework of the Grant of the President of the Russian Federation (Grant No. MK-2360.2020.2). The trapping experiments were supported by ERC StG "In Motion" (802279). V. V. F. thanks the Russian Foundation for Basic Research (RFBR project No. 19-32-60037) for support of nanowire growth.

TEM characterization studies were performed using the equipment of the Federal Joint Research Center "Material science and characterization in advanced technology" (project RFMEFI62119X0021).

References

1 L. Leandro, J. Hastrup, R. Reznik, G. Cirlin and N. Akopian, Resonant Excitation of Nanowire Quantum Dots, *npj Quantum Inf.*, 2020, **6**, 1–5, DOI: 10.1038/s41534-020-00323-9.

2 P. Krogstrup, H. I. Jørgensen, M. Heiss, O. Demichel, J. V. Holm, M. Aagesen, J. Nygard and A. Fontcuberta I

Morral, Single-Nanowire Solar Cells beyond the Shockley-Queisser Limit, *Nat. Photonics*, 2013, **7**, 306–310, DOI: 10.1038/nphoton.2013.32.

3 A. L. Falk, F. H. L. Koppens, C. L. Yu, K. Kang, N. De Leon Snapp, A. V. Akimov, M. H. Jo, M. D. Lukin and H. Park, Near-Field Electrical Detection of Optical Plasmons and Single-Plasmon Sources, *Nat. Phys.*, 2009, **5**(7), 475–479, DOI: 10.1038/nphys1284.

4 L. Cao, J. S. White, J. S. Park, J. A. Schuller, B. M. Clemens and M. L. Brongersma, Engineering Light Absorption in Semiconductor Nanowire Devices, *Nat. Mater.*, 2009, **8**(8), 643–647, DOI: 10.1038/nmat2477.

5 T. Kuykendall, P. Ulrich, S. Aloni and P. Yang, Complete Composition Tunability of InGaN Nanowires Using a Combinatorial Approach, *Nat. Mater.*, 2007, **6**, 951–956, DOI: 10.1038/nmat2037.

6 E. Roche, Y. André, G. Avit, C. Bougerol, D. Castelluci, F. Réveret, E. Gil, F. Médard, J. Leymarie, T. Jean, V. G. Dubrovskii and A. Trassoudaine, Circumventing the Miscibility Gap in InGaN Nanowires Emitting from Blue to Red, *Nanotechnology*, 2018, **29**(46), 465602, DOI: 10.1088/1361-6528/aaddc1.

7 K. Y. Shugurov, A. M. Mozharov, A. D. Bolshakov, V. V. Fedorov, G. A. Sapunov, I. V. Shtrom, A. V. Uvarov, D. A. Kudryashov, A. I. Baranov, V. Yu Mikhailovskii, V. V. Neplokh, M. Tchernycheva, G. E. Cirlin and I. S. Mukhin, Hydrogen Passivation of the N-GaN Nanowire/p-Si Heterointerface, *Nanotechnology*, 2020, **31**(24), 244003, DOI: 10.1088/1361-6528/ab76f2.

8 L. J. Lauhon, M. S. Gudiksen and C. M. Lieber, Semiconductor Nanowire Heterostructures, *Philos. Trans. R. Soc., A*, 2004, **362**(1819), 1247–1260, DOI: 10.1098/rsta.2004.1377.

9 S. Ambrosini, M. Fanetti, V. Grillo, A. Franciosi and S. Rubini, Self-Catalyzed GaAs Nanowire Growth on Si-Treated GaAs(100) Substrates, *J. Appl. Phys.*, 2011, **109**, 094306, DOI: 10.1063/1.3579449.

10 K. Schneider, P. Welter, Y. Baumgartner, H. Hahn, L. Czornomaz and P. Seidler, Gallium Phosphide-on-Silicon Dioxide Photonic Devices, *J. Lightwave Technol.*, 2018, **36**(14), 2994–3002, DOI: 10.1109/JLT.2018.2829221.

11 D. O'Mahony, M. N. Hossain, J. Justice, E. Pelucchi, A. O'Riordan, B. Roycroft and B. Corbett, High Index Contrast Optical Platform Using Gallium Phosphide on Sapphire: An Alternative to SOI?, in *Silicon Photonics and Photonic Integrated Circuits III*, 2012, vol. 8431. DOI: 10.1117/12.922687.

12 V. Neplokh, F. M. Kochetkov, K. V. Deriabin, V. V. Fedorov, A. D. Bolshakov, I. E. Eliseev, V. Y. Mikhailovskii, D. A. Ilatovskii, D. V. Krasnikov, M. Tchernycheva, G. E. Cirlin, A. G. Nasibulin, I. S. Mukhin and R. M. Islamova, Modified Silicone Rubber for Fabrication and Contacting of Flexible Suspended Membranes of N-/p-GaP Nanowires with a Single-Walled Carbon Nanotube Transparent Contact, *J. Mater. Chem. C*, 2020, **8**(11), 3764–3772, DOI: 10.1039/c9tc06239d.

13 A. Ashkin, Acceleration and Trapping of Particles by Radiation Pressure, *Phys. Rev. Lett.*, 1970, **24**(4), 156–159, DOI: 10.1103/PhysRevLett.24.156.

14 K. Svoboda and S. M. Block, Biological Applications of Optical Forces, *Annu. Rev. Biophys. Biomol. Struct.*, 1994, **23**(1), 247–285, DOI: 10.1146/annurev.bb.23.060194.001335.

15 M. L. Juan, M. Righini and R. Quidant, Plasmon Nano-Optical Tweezers, *Nat. Photonics*, 2011, **5**(6), 349–356, DOI: 10.1038/nphoton.2011.56.

16 H. Markovich, I. I. Shishkin, N. Hendler and P. Ginzburg, Optical Manipulation along an Optical Axis with a Polarization Sensitive Meta-Lens, *Nano Lett.*, 2018, **18**(8), 5024–5029, DOI: 10.1021/acs.nanolett.8b01844.

17 A. Ivinskaya, N. Kostina, A. Proskurin, M. I. Petrov, A. A. Bogdanov, S. Sukhov, A. V. Krasavin, A. Karabchevsky, A. S. Shalin and P. Ginzburg, Optomechanical Manipulation with Hyperbolic Metasurfaces, *ACS Photonics*, 2018, **5**(11), 4371–4377, DOI: 10.1021/acsphotonics.8b00775.

18 P. J. Pauzauskie, A. Radenovic, E. Trepagnier, H. Shroff, P. Yang and J. Liphardt, Optical Trapping and Integration of Semiconductor Nanowire Assemblies in Water, *Nat. Mater.*, 2006, **5**, 97–101, DOI: 10.1038/nmat1563.

19 R. Agarwal, K. Ladavac, Y. Roichman, G. Yu, C. M. Lieber and D. G. Grier, Manipulation and Assembly of Nanowires with Holographic Optical Traps, *Opt. Express*, 2005, **13**(22), 8906–8912, DOI: 10.1364/opex.13.008906.

20 Y. Nakayama, P. J. Pauzauskie, A. Radenovic, R. M. Onorato, R. J. Saykally, J. Liphardt and P. Yang, Tunable Nanowire Nonlinear Optical Probe, *Nature*, 2007, **447**, 1098–1101, DOI: 10.1038/nature05921.

21 F. Dutto, C. Raillon, K. Schenk and A. Radenovic, Nonlinear Optical Response in Single Alkaline Niobate Nanowires, *Nano Lett.*, 2011, **11**(6), 2517–2521, DOI: 10.1021/nl201085b.

22 P. J. Reece, S. Paiman, O. Abdul-Nabi, Q. Gao, M. Gal, H. H. Tan and C. Jagadish, Combined Optical Trapping and Microphotoluminescence of Single InP Nanowires, *Appl. Phys. Lett.*, 2009, **95**, 101109, DOI: 10.1063/1.3225148.

23 F. Wang, P. J. Reece, S. Paiman, Q. Gao, H. H. Tan and C. Jagadish, Nonlinear Optical Processes in Optically Trapped InP Nanowires, *Nano Lett.*, 2011, **11**(10), 4149–4153, DOI: 10.1021/nl2020262.

24 P. Trofimov, A. P. Pushkarev, I. S. Sinev, V. V. Fedorov, S. Bruyère, A. Bolshakov, I. S. Mukhin and S. V. Makarov, Perovskite-Gallium Phosphide Platform for Reconfigurable Visible-Light Nanophotonic Chip, *ACS Nano*, 2020, **14**(7), 8126–8134, DOI: 10.1021/acsnano.0c01104.

25 V. Tassev, M. Snure, R. Peterson, K. L. Schepler, R. Bedford, M. Mann, S. Vangala, W. Goodhue, A. Lin, J. Harris, M. Fejer and P. Schunemann, Progress in Orientation-Patterned GaP for next-Generation Nonlinear Optical Devices, in *Nonlinear Frequency Generation and Conversion: Materials, Devices, and Applications XII*, 2013, vol. 8604. DOI: 10.1117/12.2008057.

26 P. Ginzburg, A. Krasavin, Y. Sonnefraud, A. Murphy, R. J. Pollard, S. A. Maier and A. V. Zayats, Nonlinearly

Coupled Localized Plasmon Resonances: Resonant Second-Harmonic Generation, *Phys. Rev. B: Condens. Matter Mater. Phys.*, 2012, **86**, 085422, DOI: 10.1103/PhysRevB.86.085422.

27 R. Sanatinia, S. Anand and M. Swillo, Modal Engineering of Second-Harmonic Generation in Single GaP Nanopillars, *Nano Lett.*, 2014, **14**(9), 5376–5381, DOI: 10.1021/nl502521y.

28 D. P. Lake, M. Mitchell, H. Jayakumar, L. F. Dos Santos, D. Curic and P. E. Barclay, Efficient Telecom to Visible Wavelength Conversion in Doubly Resonant Gallium Phosphide Microdisks, *Appl. Phys. Lett.*, 2016, **108**, 031109, DOI: 10.1063/1.4940242.

29 R. Sanatinia, M. Swillo and S. Anand, Surface Second-Harmonic Generation from Vertical GaP Nanopillars, *Nano Lett.*, 2012, **12**(2), 820–826, DOI: 10.1021/nl203866y.

30 O. Y. Koval, V. V. Fedorov, A. D. Bolshakov, S. V. Fedina, F. M. Kochetkov, V. Neplokh, G. A. Sapunov, L. N. Dvoretckaia, D. A. Kirilenko, I. V. Shtrom, R. M. Islamova, G. E. Cirlin, M. Tchernycheva, A. Y. Serov and I. S. Mukhin, Structural and Optical Properties of Self-Catalyzed Axially Heterostructured GaPN/GaP Nanowires Embedded into a Flexible Silicone Membrane, *Nanomaterials*, 2020, **10**(11), 1–15, DOI: 10.3390/nano10112110.

31 O. Y. Koval, V. V. Fedorov, A. D. Bolshakov, I. E. Eliseev, S. V. Fedina, G. A. Sapunov, S. A. Udovenko, L. N. Dvoretckaia, D. A. Kirilenko, R. G. Burkovsky and I. S. Mukhin, Xrd Evaluation of Wurtzite Phase in Mbe Grown Self-Catalyzed Gap Nanowires, *Nanomaterials*, 2021, **11**(4), 960, DOI: 10.3390/nano11040960.

32 X. Guo, Y. Ying and L. Tong, Photonic Nanowires: From Subwavelength Waveguides to Optical Sensors, *Acc. Chem. Res.*, 2014, **47**(2), 656–666, DOI: 10.1021/ar400232h.

33 A. D. Bolshakov, L. N. Dvoretckaia, V. V. Fedorov, G. A. Sapunov, A. M. Mozharov, K. Y. Shugurov, V. A. Shkoldin, M. S. Mukhin, G. E. Cirlin and I. S. Mukhin, Microlens-Enhanced Substrate Patterning and MBE Growth of GaP Nanowires, *Semiconductors*, 2018, **52**, 2088–2091, DOI: 10.1134/S1063782618160054.

34 A. Martin, S. Combrié, A. de Rossi, G. Beaudoin, I. Sagnes and F. Raineri, Nonlinear Gallium Phosphide Nanoscale Photonics [Invited], *Photonics Res.*, 2018, **6**(5), B43–B49, DOI: 10.1364/prj.6.000b43.

35 A. D. Bolshakov, V. V. Fedorov, N. V. Sibirev, M. V. Fetisova, E. I. Moiseev, N. V. Kryzhanovskaya, O. Y. Koval, E. V. Ubyivovk, A. M. Mozharov, G. E. Cirlin and I. S. Mukhin, Growth and Characterization of GaP/GaPAs Nanowire Heterostructures with Controllable Composition, *Phys. Status Solidi RRL*, 2019, **13**(11), 1900350, DOI: 10.1002/pssr.201900350.

36 V. V. Fedorov, Y. Berdnikov, N. V. Sibirev, A. D. Bolshakov, S. V. Fedina, G. A. Sapunov, L. N. Dvoretckaia, G. Cirlin, D. A. Kirilenko, M. Tchernycheva and I. S. Mukhin, Tailoring morphology and vertical yield of self-catalyzed GaP nanowires on template-free Si substrates, *Nanomaterials*, 2021, **11**(8), 1949.

37 R. W. G. Wyckoff, *Crystal structures (Vol. 1, p. 312)*, Interscience publishers, New York, 1963.

38 V. G. Dubrovskii and N. V. Sibirev, Growth Thermodynamics of Nanowires and Its Application to Polytypism of Zinc Blende III-V Nanowires, *Phys. Rev. B: Condens. Matter Mater. Phys.*, 2008, **77**, 035414, DOI: 10.1103/PhysRevB.77.035414.

39 V. V. Fedorov, A. Bolshakov, O. Sergaeva, V. Neplokh, D. Markina, S. Bruyere, G. Saerens, M. I. Petrov, R. Grange, M. Timofeeva, S. V. Makarov and I. S. Mukhin, Gallium Phosphide Nanowires in a Free-Standing, Flexible, and Semitransparent Membrane for Large-Scale Infrared-to-Visible Light Conversion, *ACS Nano*, 2020, **14**(8), 10624–10632, DOI: 10.1021/acsnano.0c04872.

40 S. Gradečak, F. Qian, Y. Li, H. G. Park and C. M. Lieber, GaN Nanowire Lasers with Low Lasing Thresholds, *Appl. Phys. Lett.*, 2005, **87**, 173111, DOI: 10.1063/1.2115087.

41 A. V. Krasavin, P. Ginzburg and A. V. Zayats, Free-Electron Optical Nonlinearities in Plasmonic Nanostructures: A Review of the Hydrodynamic Description, *Laser Photonics Rev.*, 2018, **12**(1), 1700082, DOI: 10.1002/lpor.201700082.

42 P. Segovia, G. Marino, A. V. Krasavin, N. Olivier, G. A. Wurtz, P. A. Belov, P. Ginzburg and A. V. Zayats, Hyperbolic Metamaterial Antenna for Second-Harmonic Generation Tomography, *Opt. Express*, 2015, **23**(24), 30730, DOI: 10.1364/OE.23.030730.